

1 Comparison of physical and chemical properties of ambient aerosols
2 during the 2009 haze and non-haze periods in Southeast Asia

3 Jingsha Xu^{1,2}, Xuhong Tai³, Raghu Betha³, Jun He ^{2*}, Rajasekhar Balasubramanian^{3§}

4

5 ¹ International Doctoral Innovation Centre, The University of Nottingham Ningbo
6 China, Ningbo 315100, China

7 ² Department of Chemical and Environmental Engineering, The University of
8 Nottingham Ningbo China, Ningbo 315100, China

9 ³ Department of Civil and Environmental Engineering, National University of
10 Singapore, Singapore

11

12 Correspondence to:

13 *Dr Jun He at: jun.he@nottingham.edu.cn or

14 §Dr Rajasekhar Balasubramanian at: ceerbala@nus.edu.sg

Abstract

15 Recurrent smoke haze episodes that occur in Southeast Asia (SEA) are of much
16 concern because of their environmental and health impacts. These haze episodes are
17 mainly caused by uncontrolled biomass and peat burning in Indonesia. Airborne
18 particulate matter (PM) samples were collected in the Southwest (SW) coast of
19 Singapore from 16 August to 9 November in 2009 to assess the impact of smoke haze
20 episodes on the air quality due to the long-range transport of biomass and peat
21 burning emissions., The physical and chemical characteristics of PM were
22 investigated during pre-haze, smoke-haze, and post-haze periods. Days with PM_{2.5}
23 mass concentrations of $\geq 35 \mu\text{g m}^{-3}$ were considered as smoke-haze events. Using this
24 criterion, out of the total 82 sampling days, 9 smoke-haze events were identified. The
25 origin of air masses during smoke haze episodes was studied on the basis of
26 HYPPLIT backward air trajectory analysis for 4 days. In terms of the physical
27 properties of PM, higher particle surface area concentrations (PSAC) and particle
28 gravimetric mass concentrations (PGMC) were observed during the smoke-haze
29 period, but there was no consistent pattern for particle number concentrations (PNC)
30 during the haze period as compared to the non-haze period except that there was a
31 significant increase at about 08:00, which could be attributed to the entrainment of
32 PM from aloft after the break-down of the nocturnal inversion layer. As for the
33 chemical characteristics of PM, among the six key inorganic water-soluble ions (Cl⁻,
34 NO₃⁻, nss-SO₄²⁻, Na⁺, NH₄⁺, and nss-K⁺) measured in this study, NO₃⁻, nss-SO₄²⁻, and
35 NH₄⁺ showed a significant increase in their concentrations during the smoke-haze
36 period together with nss-K⁺. These observations suggest that the increased
37 atmospheric loading of PM with higher surface area and increased concentrations of
38 optically active secondary inorganic aerosols (NH₄)₂SO₄ or NH₄HSO₄ and NH₄NO₃)
39 resulted in the atmospheric visibility reduction in SEA due to the advection of
40 biomass and peat burning emissions.

41

42 **Keywords:** Haze aerosol · Biomass burning · Physical properties · Inorganic ions.

43 **Introduction**

44 Atmospheric haze (reduced visibility), caused by increased loading of aerosols, has a
45 strong impact on the radiative balance of the Earth by direct reflection and absorption
46 of incoming solar radiation or by indirect reflection due to cloud formation (IPCC
47 2007; Jacobson 2004; Pandis and Seinfeld 1998). It is known that the haze
48 phenomenon is caused by either natural sources such as volcanic eruptions and
49 naturally ignited fires, or anthropogenic sources such as fossil fuel related combustion,
50 uncontrolled biomass burning, biofuel burning, land use changes for agriculture or
51 developments, or a combination of both (He et al. 2010; Jacobson 2004). The
52 chemical composition of haze aerosols depends largely on the fuel type, combustion
53 phase (flaming vs. smoldering), duration and intensity of combustion, and prevailing
54 meteorological conditions (Reid et al. 2005). Generally, haze aerosols contain both
55 primary particulates emitted directly into the atmosphere and secondary particulates
56 formed from gaseous precursors emitted, the relative proportion of which would
57 change over time and distance. Although the general residence time of ambient fine
58 aerosols is usually > 5 days, at about 1 to 2 weeks with age, it is still much shorter
59 than that of greenhouse gases. Nevertheless, the average transport distance over which
60 aerosols are transported is estimated to be ≥ 1000 km, leading to potentially large
61 regions that can be affected by the influence of haze when there is extensive biomass
62 burning over a wide area (Brook et al. 2007).

63 Smoke haze episodes occur in Southeast Asia (SEA) annually due to recurrent
64 slash and burn agricultural activities, but with different intensities and impacts from
65 year to year depending on weather conditions. As SEA's air quality is influenced by
66 local particle emissions heavily, the SEA haze becomes a complex regional air
67 pollution problem, due to the intermixing of haze particles with fossil fuel-derived
68 particles, with the following impacts. The physical, chemical and optical properties of
69 the SEA haze can affect the ecosystems, human health, climate change and water
70 budget in the affected regions (Ramanathan et al. 2005; Sundarambal et al. 2010).
71 The reduction of atmospheric visibility can vary from 20% to 90% depending on the
72 intensity of haze episodes and the characteristics of aerosols contained in them
73 (Wang 2002). Severe smoke-haze episodes can also indirectly affect the efficiency of
74 vegetative photosynthesis. When water insoluble aerosols deposited on leaves are not
75 washed off by precipitation, they could lead to a reduction of as much as 35%

76 photosynthesis with lower crop yields, lesser CO₂ removal and eventual increase in
77 greenhouse effects (Bergin et al. 2001; Tang 1996). In terms of regional climate
78 change, with the high emission of light absorbing aerosol particulates into the
79 atmosphere, greenhouse effects are expected to increase due to the concurrent
80 increase of greenhouse gases emitted, even when the aerosol's short-term cooling
81 effects are considered in the radiative budget (Jacobson 2004). The massive
82 concurrent emissions of CO₂ from biomass burning together with aerosols have been
83 linked to the prolonged duration of the regional La Nina effects (unusually cold and
84 wet weather conditions in SEA) (Van der Werf 2008). The increased smoke particle
85 concentration associated with smoke-haze episodes could also affect cloud cover and
86 the cloud chemistry (Geresdi et al. 2006; Reid et al. 2005). Strong associations
87 between increased aerosol concentrations and health effects have been observed
88 during the regional smoke-haze episodes over the years. On average, a nearly six fold
89 increase in emergency visits for acute asthma exacerbation were observed for every
90 20 µg m⁻³ increase of the total suspended particles (TSP) from 78 µg m⁻³ (Chew et al.
91 1999).

92 Dry weather conditions in SEA over the months of June to October 2009,
93 exacerbated by the El Niño Southern Oscillation (ENSO), increased the likelihood of
94 massive uncontrolled burning due to prolonged droughts (Gnanaseelan and Vaid 2010;
95 Aiken 2004). The sampling site was influenced by the southwest (SW) winds from
96 August to October. In view of a range of environmental and health impacts associated
97 with smoke-haze periods, it is important to characterize the physical and chemical
98 properties of haze and non-haze aerosols in SEA so that appropriate environmental
99 policies and practical mitigation strategies can be developed to protect sensitive
100 ecosystems and human health. Therefore, a field sampling campaign was conducted in
101 the Southwest (SW) coast of Singapore from 16 August to 9 November in 2009. This
102 study aimed at investigating both physical and chemical properties of haze aerosols in
103 relation to those of background aerosols. In addition, backward trajectory analysis was
104 carried out to assess the influence of air masses of different origins on the aerosol
105 physical and chemical properties as well.

106

107 **Methods**

108 Sample Collection

109 Particulate sampling was carried out from 16 August 2009 to 9 November 2009,
110 beginning at 09:00 (UTC+8 hrs) till the following day. The sampling site (1° 18' N,
111 103° 46' E) is located at an altitude of 67 m above sea level at the roof of block E2 in
112 the National University of Singapore (NUS). Singapore (1° 18' N, 103° 50' E) is
113 situated at the tip of Peninsula Malaysia and within the regional influences of SEA
114 smoke-haze with a total area of 693 km². The sampling site is considered to be an
115 urban background location where the local air quality is influenced largely by
116 vehicular traffic on the major expressway (Ayer Rajah Expressway) and industrial
117 emissions from petroleum, petrochemical, and specialty chemical industries located
118 on Jurong Island, 5 to 10 km on the southwest of this site. The sampling site is also
119 influenced by the long-range transport of smoke-haze impacted air masses from
120 Sumatra, Indonesia (Balasubramanian et al. 2003; Balasubramanian et al. 1999).

121 PM_{2.5} were collected by 2 Mini-Vol Portable Samplers (MPSs) (AirMetrics, US)
122 running in parallel with Teflon membrane filters at the flow rate of 6 Lmin⁻¹ for 24-
123 hrs. The filter sample collection was performed periodically in every 1-in-6 days with
124 additional sample collections performed when smoke-haze episodes were observed.
125 Before and after the sampling, all the filters were equilibrated under the conditions
126 with 22 ± 1°C with controlled relative humidity (RH) of 35% for 24 hours right
127 before they were weighed with a MC5 microbalance (Sartorius AG) accurate to 1µg.
128 Meanwhile, subsets of both filters were stored and analyzed as laboratory blanks.

129 Physical Measurements of Atmospheric Aerosols

130 The particle number concentration and size distribution were measured by a real-time
131 Fast Mobility Particle Sizer (FMPS, TSI-3091d, TSI.) with a mobility diameter range
132 of 5.6 to 560 nm, which is able to scan the number concentration of a poly-disperse,
133 heterogeneous aerosol particle system for the nuclei and accumulation (sub-micron)
134 mode based upon electrical-based measurements for particle counting. Data were
135 recorded every second throughout the sampling period. TSI Dust Track™ II Aerosol
136 Monitor was utilized to measure the real-time mass concentration of PM_{2.5}
137 atmospheric particles by photometric measurements based on the Mie scattering
138 theory. The Dust Track device was calibrated with reference to the gravimetric data

139 obtained from the MPS operated in parallel for a duration of 30-days using Teflon
140 membrane filters. Twice daily auto zero checks were performed with filtered
141 atmospheric air to reduce background noise influences. The Dust Track device was
142 operated at a flow rate of 3.0 L min⁻¹, and the recorded data were analyzed at 5-min
143 averages. The accuracy of the Dust Track measurements was improved by eliminating
144 positive artefacts of photometric measurements due to water vapor (Jakubczyk et al.
145 2005; Ter-Avetisyan et al. 2003). With a reasonable correlation of 0.446 and R² of
146 0.82, the collected data from the Dust Track device was classified and analyzed for
147 both smoke-haze and non-haze periods.

148 Chemical Analysis of Atmospheric Aerosols

149 Three-quarters of the Telfon filter was extracted by ultra-sonication (Elmasonic, S
150 60H) with 12 ml of ultra-pure deionized water and the extract was filtered through
151 Target® 30 mm syringe filters with 0.45 µm Teflon membrane.. After this step, the
152 extracts were processed for the Ion Chromatography(IC) analysis. All filter samples
153 extracted and the ones remaining after chemical analysis were stored in individual
154 vials at 4°C for future analysis. In this study, six inorganic ions from the aerosol
155 extracts: Cl⁻, NO₃⁻, SO₄²⁻, Na⁺, NH₄⁺ and K⁺ were quantified by the Ion
156 Chromatography (Dionex ICS-2000) and the detection is based on the concept of
157 conductivity detection of either anions or cations by suppression, separated over
158 individual retention times.

159 Air Mass Backward Trajectory Analysis

160 The latest, updated Hybrid Single-Particle Lagrangian Integrated Trajectory
161 (HYSPLIT) model (Version 4.9) (Draxler 2013; Rolph 2013), developed by the
162 National Oceanic and Atmospheric Administration (NOAA), was used to compute
163 backward trajectories for air samples collected in this study. Meteorological data were
164 obtained from National Centers for Environmental Prediction (NCEP) Global Data
165 Assimilation System (GDAS, global, 2006-present). Kinematic 3D trajectories were
166 used as they are reported to provide an accurate description of the history of air
167 masses in comparison with all of the other approaches (isentropic, isobaric) (Stohl
168 1998; Stohl and Seibert 1998). Backward air trajectories, beginning at 09:00, were
169 generated at every 6-hrs intervals during each sampling event for 96 h back in time
170 with 500 m-agl ending level. This atmospheric level is very frequently used (Erel et al.

171 2007; Lee et al. 2006) and ensures that the trajectory starts in the atmospheric
172 boundary layer (ABL) (Dvorska et al. 2009). In addition, cluster analysis was
173 conducted by using HYSPLIT model (version 4.9) as well to classify the trajectory
174 groups of similar length and curvature for monsoon and pre-monsoon seasons.

175 Quality Control

176 Inconsistency in MPS measurements was verified by concurrent sampling of multiple
177 MPSs and the comparison of the collected aerosol masses. A range of about ± 5 to 10%
178 mass difference can be considered acceptable between MPS collections. During the
179 entire sampling period, the filters were placed in individual polystyrene petri dishes,
180 and handled with stainless-steel forceps, housed under an air-conditioned environment
181 set at an average 22°C in the laboratory. After post-gravimetric analysis, filters were
182 stored at -15°C until extraction and chemical analysis so as to prevent contamination
183 and degradation. Quality control for the IC analysis was performed by running a
184 series of calibration standards in step-up concentrations. An intermediate analysis of
185 the median calibration standard was performed after analysis of every 24 samples to
186 ensure stability and consistency of the IC accuracy. Duplicates were also performed to
187 ensure the reproducibility of the samples of interest. Initial calibration and quality
188 checks on FMPS were undertaken regularly. These procedures would eliminate
189 interference from the instruments and give more reliable results.

190 **Results and discussion**

191 Segmentation of Clear Background Days and smoke-haze Events

192 From the analysis of the meteorological parameters acquired from the automated
193 weather station deployed at the sampling site, it became clear that there was very little
194 variation in pressure, air temperature, relative humidity and rainfall during the
195 sampling period. These climate conditions with little variations throughout the year
196 are quite typical in tropical countries such as Singapore (Betha et al. 2013).

197 Out of the 82 sampling days for the daily average Dust Track-corrected
198 gravimetric mass concentration, 9 days were identified as hazy days when the 24-hr
199 average PM_{2.5} mass concentration was $\geq 35 \mu\text{g m}^{-3}$. Otherwise, the remaining 73 days
200 were considered to be clear days. This criterion was selected based on the analysis of
201 smoke haze events reported in our previous reports (Balasubramanian et al. 2003; See

202 et al. 2006). The same criterion was also used for identification of smoke haze events
203 in other countries. For example, Hu et al. (2008) reported the occurrence of smoke
204 haze events in Atlanta, GA, caused by prescribed forest fires, when the 24-hr
205 average PM_{2.5} mass concentration exceeded the National Ambient Air Quality
206 Standard (NAAQS) of 35 µg m⁻³ (Hu et al. 2008). Smoke haze events were also
207 identified in Malaysia using the same criterion as used in this study (Radzi bin Abas et
208 al. 2004). Figure 1 shows the classification of smoke events in this study. A general
209 pattern of variations in 24-hr average PM_{2.5} mass concentrations observed during pre-
210 haze, smoke-haze, and post-haze periods can be noticed. The pre-haze period lasted
211 from 16 August 2009 to 11 September 2009 while the smoke-haze episodes occurred
212 predominantly from mid-September to early October (12 September 2009 till 3
213 October 2009) followed by the post-haze period from early October to early
214 November (4 October 2009 till 9 November 2009). In this study, pre- and post-haze
215 periods are considered to be non-haze periods.

216 Air Mass Backward Trajectory Analysis

217 The smoke-haze air mass origins were identified based on back trajectory analysis at
218 the elevation of 500 m-agl over 96-hrs (4-days). Representative trajectories are
219 displayed in Figure 2 for the pre-haze, smoke-haze and post-haze periods.

220 As can be seen from Figure 2(a) and (d), there were only a few hotspots present
221 over the SEA region. Aerosols during the pre-haze period at Singapore might have
222 been influenced by those hotspots occurring in Indonesia as most air masses
223 originated from marine sources and passed through Java Sea before arriving at
224 Singapore. Figures 2(b) and (e), show a number of hotspots (biomass and peat-land
225 fires) located in Sumatra and the southern part of Indonesia and a cluster of back
226 trajectories representing the transport of biomass burning-impacted air masses over
227 the two regions (Sumatra and southern part of Indonesia) before reaching Singapore,
228 respectively. As can be seen from Figure 2(c), there were no visible hotspots in
229 Sumatra or Kalimantan while Figure 2(f) shows that the air masses originated from
230 partly terrestrial and partly oceanic sources during the post-haze period. Thus, the
231 satellite images and the back trajectory analysis indicated that the smoke-haze
232 episodes that occurred in Singapore from September to October 2009 were due to
233 biomass burning in Indonesia and the subsequent long-range transport of fire
234 emissions.

235 Comparison of Physical Properties of Aerosols between Non-haze and Haze Periods
236 Differences in the physical properties of aerosols between non-haze and haze affected
237 days were investigated by comparing the diurnal particle number concentrations
238 (PNC), particle surface area concentrations (PSAC), and particle gravimetric mass
239 concentrations (PGMC) as shown in Figure 3. Figures 3(a) and (b) show the
240 normalized concentrations of measured particle number ($dN/d\log D_p$) and estimated
241 surface area ($dS/d\log D_p$) concentrations during sampling days. As can be seen from
242 Figure 3(a), the average diurnal PNC was $3.31 \times 10^5 \text{ cm}^{-3}$ for clear days and 3.50×10^5
243 cm^{-3} for hazy days. For non-hazy days, four distinctive peaks were observed. For
244 smoke-haze days, the most significant peak was the one observed at 0800 hrs with the
245 highest PNC being $8.14 \times 10^5 \pm 1.29 \times 10^6 \text{ cm}^{-3}$ (mean \pm SD) and also with the largest
246 standard error due to the most severe smoke-haze episode that occurred on the 27th
247 September 2009 with the maximum PNC of $3.73 \times 10^6 \text{ cm}^{-3}$ and with the 24-hr mean
248 of $5.37 \times 10^5 \text{ cm}^{-3}$.

249 Interestingly, smoke-haze affected days had a higher PNC than that of non-hazy
250 days before 10:00. However, the PNC declined after 10:00 and became even lower
251 than that on non-hazy days. The decline in the PNC appears to be associated with the
252 pronounced vertical mixing of air in the presence of sunlight during day i.e. improved
253 advection and dispersion of haze particles. In addition, the removal of aerosol
254 particles by sedimentation or scavenging from the atmosphere is also possible (Reid et
255 al. 2005). For non-hazy and hazy days, the influence of local traffic and industrial
256 primary emissions is expected to be basically the same, but the significantly increased
257 atmospheric loading of pre-existing particles in smoke haze period can suppress the
258 occurrence of nucleation during the day by removing precursor gases through
259 adsorption (Betha et al. 2013). When relatively lower PNC was present during non-
260 haze period, the formation of new particles via nucleation process became favourable.
261 The competing pathways involved in the formation of new particles and the removal
262 of “aged” pre-existing particles apart from changes in atmospheric dynamics in the
263 presence of the haze layer may eventually lead to the higher number concentration of
264 particles during the daytime in the non-haze period compared to the smoke haze
265 period. We have recently reported that new particle formation (NPF) mainly occurred
266 in the afternoon (Betha et al. 2013), which may partly explain the observation of a
267 sustained high number concentration from 12:00 till 18:00 during the non-smoke

268 haze period in this study. A rapid increase in PNC observed from 15:00 to 16:00 with
269 most of the particles with diameters less than 25 nm, as shown in Figure 4, supports
270 the hypothesis about the occurrence of NPF events in the tropical atmosphere (Betha
271 et al. 2013).

272 During both non-haze and haze periods, the slight general increase of PNC in the
273 early morning hours and in the late night hours during the non-smoke haze period can
274 be attributed to the nocturnal inversion layer that formed to decrease the mixing
275 height, thus, increasing the ground-level PNC due to poor dispersion of ambient air.
276 The mixing height generally increases as the day progresses with an increase in
277 temperature. The larger fluctuations in the PNC in the early morning hours between
278 02:00 and 05:00 can potentially be due to changes in the strength of biomass burning
279 emissions from the hotspots in Indonesia and/or in the long distance transboundary
280 transport of primary aerosol particles. The distinct peak observed at 08:00 during the
281 smoke-haze period appears to be influenced by the entrainment of haze particles from
282 aloft (downward transport of haze particles from above the mixing height) when the
283 nocturnal inversion layer breaks down after the sunrise (i.e. fumigation).

284 Figures 3(b) and (c) show distinctly higher daily mean PSAC and PGMC during
285 the smoke-haze period. The mean PSAC measured was $4.75 \times 10^9 \text{ nm}^2 \text{ cm}^{-3}$ during the
286 non-haze period and $6.39 \times 10^9 \text{ nm}^2 \text{ cm}^{-3}$ during the smoke-haze period. The mean
287 PGMC measured was $12.43 \mu\text{g m}^{-3}$ during the non-haze period and $57.46 \mu\text{g m}^{-3}$
288 during the smoke-haze period. However, with the measurement of PNC by the FMPS
289 being in the range of 5.6 to 560nm, the PSAC measurements were only made in the
290 ultra-fine and sub-micron range. The PSAC peaks observed at 08:00, 12:00 and 17:00
291 during the non-hazy period, and also the peaks observed at 08:00 and 19:00 hours
292 during the smoke-haze period can potentially be associated with the diurnal emission
293 variations of local rush hour traffic emissions in the case of the non-haze period and a
294 mix of local particulate emissions and transboundary aerosol particles on hazy days.
295 These diurnal patterns were commonly reported in previous studies of the urban
296 atmosphere (e.g. Granada, Spain) by Lyamani et al. (2008).

297 A statistical summary of PNC and PSAC measured during the non-haze (the pre-
298 and post-haze periods) and the haze periods is given in Table 1 for different particle
299 size ranges, namely the key nuclei mode from 0 to 50 nm, the ultrafine particle mode
300 from 51 to 100 nm, and part of the submicron, accumulation particle mode from 101
301 to 560 nm. As can be seen from the table the mean PNC measured during the haze

302 period was significantly higher than that during the non-haze period in the particle
303 size range of 51-100 nm, while the mean PSAC calculated for hazy days is smaller
304 than that for non-hazy days in the particle size range of 0-100 nm, but almost twice
305 higher than that in the range of 101-560 nm for non-hazy days. This observation
306 suggests that the aerosol particles in the size range of 101-560 nm absorbed and/or
307 scattered the incoming sunlight efficiently because of the higher surface area and thus
308 contributed to atmospheric visibility reduction i.e. haze

309 Comparison of Chemical Properties of Aerosols between Non-haze and Haze Periods

310 Chemical characteristics of aerosols measured between non-haze and haze periods
311 were compared and are summarized in Table 2. The proportion of the particulate-
312 bound inorganic water-soluble ions: Cl^- , NO_3^- , nss-SO_4^{2-} , Na^+ , NH_4^+ and nss-K^+ was
313 observed to be quite similar between pre- and post-haze periods. The major
314 contributors to the particulate mass over the non-haze period were mainly Cl^- , nss-
315 SO_4^{2-} , and Na^+ . A high proportion of Cl^- and Na^+ may potentially be derived in the
316 form of sea salt from the open sea which is only 800 to 1000 m away from the
317 sampling site. The presence of a high proportion of nss-SO_4^{2-} in the background air
318 during the clear days suggests that it could be produced the atmospheric pathways
319 involving the oxidation of SO_2 emitted from fossil fuel burning. This production
320 pathway is conceivable since the sampling site is located in an urban area whose air
321 quality is influenced by local traffic and industrial emissions. The non-sea salt sulfate
322 (nss-SO_4^{2-}) was calculated as follows (Balasubramanian et al. 2003).

323

$$324 \quad \text{nss} - \text{SO}_4^{2-} = [\text{SO}_4^{2-}] - [\text{Na}^+] \times 0.2516 \quad (1)$$

325 During the smoke-haze period, high mass concentrations of nss-SO_4^{2-} , NO_3^- , and
326 NH_4^+ were observed, suggesting that these secondary inorganic aerosols were
327 produced in the atmosphere under favourable conditions due to emissions of precursor
328 gases from biomass burning in Indonesia (Behera et al, 2013). These places are
329 probable locations where the peat rich grounds would provide fertile soil for future
330 agricultural land use and motivated the recurring slash-and-burn agricultural practices
331 in SEA. These findings are consistent with our previous observations during smoke-
332 haze periods (Balasubramanian et al. 1999; He and Balasubramanian 2008).
333 Indonesian peat bogs, located in Sumatra where most hotspots were identified in this

334 study, continue to smolder under several meters of land surface, especially during dry
335 spells (Gras et al. 1999; Langmann and Graf 2003), releasing chemically reactive
336 trace gases such as SO₂, NO_x and NH₃ into the atmosphere. SO₂ and NO_x are then
337 oxidized in the atmosphere and form (NH₄)₂SO₄ or NH₄HSO₄ and NH₄NO₃ in the
338 presence of NH₃ under thermodynamically favourable conditions (Behera and
339 Balasubramanian, 2014). Moreover, the oxidation products, H₂SO₄ and HNO₃ vapors,
340 can also bind themselves to pre-existing primary aerosols forming internally mixed
341 smoke plumes, leading to an increase in particle size and mass concentration (See et
342 al. 2006).

343 An increase in the inorganic water-soluble nss-K⁺ was also observed during the
344 smoke haze period. Being a chemical tracer for biomass (wood) and peat burning, the
345 increase in the concentration of nss-K⁺ further provide support in favour of the
346 influences of biomass burning on the chemical composition of smoke-haze impacted
347 aerosol particles (Currie et al. 1994). The nss-K⁺ concentration was calculated from
348 the Equation (2) below (Balasubramanian et al. 2003), and it was about 81.7 % of the
349 total inorganic water-soluble K⁺ concentration.

350

$$351 \quad \text{nss} - \text{K}^+ = [\text{K}^+] - [\text{Na}^+] \times 0.037 \quad (2)$$

352 Significant increments in the concentration of certain particulate-bound chemical
353 components were observed during the smoke-haze period compared to that during the
354 pre-haze period: NO₃⁻ (50 %), nss-SO₄²⁻ (74 %), Na⁺ (41 %), K⁺ (20%) and NH₄⁺ (3
355 fold increase). A similar increase in their concentrations was observed based on the
356 data obtained during the post-haze period, with the exception of K⁺. The Cl⁻
357 concentration was observed to be relatively stable throughout the sampling period as
358 it is mainly derived from the nearby marine sources. Thus, the enhancement in the
359 concentrations of secondary inorganic aerosols (NH₄)₂SO₄ or NH₄HSO₄ and NH₄NO₃)
360 appears to be associated with the long-range transboundary transport of biomass and
361 peat burning emissions from Sumatra to Singapore. Apart from the HYSPLIT back
362 trajectory analysis, the increase in K⁺, as a biomass burning tracer, from pre-haze to
363 smoke-haze periods can further support the above hypothesis.

364 **Conclusions**

365 In this study, smoke-haze episodes, caused by biomass and peat burning in Indonesia
366 (Sumatra), were observed predominantly during the SW monsoon which lasted from
367 12 September 2009 to 3 October 2009. While comparing the physical characteristics
368 of ambient aerosol particles between smoke-haze and non-haze periods, higher PSAC
369 and PGMC were observed along with possible particle growth (aerosol aging).
370 However, the diurnal trends in PNC showed a different pattern compared to those of
371 PSAC and PGMC. The new particle formation phenomenon which was significant
372 during the afternoons on non-haze days was suppressed during the smoke-haze
373 affected period. The mean PNC trends was observed to peak at 07:00 to 09:00 and
374 17:00 to 19:00 due to local emissions from rush hour traffic during both smoke-haze
375 and non-haze periods. However, a significant peak was observed in the background
376 air in the absence of smoke haze at about 15:00 to 16:00 which could be attributed to
377 NPF. Generally, the overall mean PNC, PSAC and PGMC measured during the
378 smoke-haze period were higher than those during the non-hazy period. Among the 6
379 key particulate-bound inorganic ions investigated in this study, NH_4^+ and SO_4^{2-}
380 were observed to have the largest increase in their concentrations during the smoke
381 haze period compared to their measurements during the non-haze period. K^+ , a well-
382 known chemical tracer of biomass and peat burning, was observed to have increased
383 in its concentration during the smoke-haze period compared to the pre-haze period.
384 This observation together with the back trajectory analysis suggests that the long-
385 range transport of biomass and peat burning emissions from Indonesia to Singapore
386 affects both the physical and chemical characteristics of aerosol particles at downwind
387 sites. In addition, the increase in surface area of aerosols in the range of 101-560 nm
388 together with the increase in the concentration of radiatively active secondary
389 inorganic aerosols ($(\text{NH}_4)_2\text{SO}_4$ or NH_4HSO_4 and NH_4NO_3) is indicative of the
390 contribution of these particles to atmospheric visibility reduction during the smoke
391 haze period. With the repeated occurrence of smoke haze episodes in SEA, there is a
392 possibility of inducing climate change on a regional scale, which in turn could affect
393 the hydrological cycle and thus the water budget.

394 **Acknowledgements**

395 The authors acknowledge the financial support from Ningbo Education Bureau,
396 Ningbo Science and Technology Bureau, China's MOST and The University of

397 Nottingham. The work is also partially supported by EPSRC grant no. EP/L016362/1,
398 Chinese National Natural Science Foundation (41303091) and Ningbo Municipal
399 Natural Science Foundation (2014A610096).

400 REFERENCES

- 401 Aiken, S. R. (2004). Runaway Fires, Smoke-haze Pollution, and Unnatural Disasters in Indonesia.
402 *Geographical Review*, 94:55-79.
- 403 Balasubramanian, R., Qian, W. B., Decesari, S., Facchini, M. C., & Fuzzi, S. (2003). Comprehensive
404 characterization of PM_{2.5} aerosols in Singapore. *Journal of Geophysical Research-Atmosphere*, 108
405 (D16):4523, doi:10.1029/2002jd002517.
- 406 Balasubramanian, R., Victor, T., & Begum, R. (1999). Impact of biomass burning on rainwater acidity
407 and composition in Singapore. *Journal of Geophysical Research-Atmosphere*, 104(D21): 26881-
408 26890 , doi:10.1029/1999jd900247.
- 409 Bergin, M. H., Greenwald, R., Xu, J., Berta, Y., & Chameides, W. L. (2001). Influence of aerosol dry
410 deposition on photosynthetically active radiation available to plants: A case study in the Yangtze
411 delta region of China. *Geophysical Research Letters*, 28(18): 3605-3608,
- 412 Behera. S.N., Betha, R., Balasubramanian, R. (2013) Insights into chemical coupling among acidic
413 gases, ammonia and secondary inorganic aerosols. *Aerosol and Air Quality Research*, 13: 1282 –
414 1296.
- 415 Behera SN and Balasubramanian, R. (2014) Influence of Biomass Burning on Temporal and Diurnal
416 Variations of Acidic Gases, Particulate Nitrate, and Sulfate in a Tropical Urban Atmosphere.
417 *Advances in Meteorology*, DOI: 10.1155/2014/828491.
- 418 Betha, R., Spracklen, D. V., & Balasubramanian, R. (2013). Observations of new aerosol particle
419 formation in a tropical urban atmosphere. *Atmospheric Environment*, 71: 340-351.
- 420 Bodhaine, B. A., Ahlquist, N. C., & Schnell, R. C. (1991). Three-wavelength nephelometer suitable for
421 aircraft measurement of background aerosol scattering coefficient. *Atmospheric Environment*,
422 25(10): 2267-2276.
- 423 Brook, J. R., Poirot, R. L., Dann, T. F., Lee, P. K. H., Lillyman, C. D., & Ip, T. (2007). Assessing
424 sources of PM_{2.5} in cities influenced by regional transport. *Journal of Toxicology and*
425 *Environmental Health-Part a-Current Issues*, 70(3-4): 191-199.
- 426 Chew, F. T., Goh, D. Y. T., Ooi, B. C., Saharom, R., Hui, J. K. S., & Lee, B. W. (1999). Association of
427 ambient air-pollution levels with acute asthma exacerbation among children in Singapore. *Allergy*,
428 54(4): 320-329.
- 429 Currie, L. A., Klouda, G. A., Klinedinst, D. B., Sheffield, A. E., Jull, A. J. T., Donahue, D. J., et al.
430 (1994). Fossil-mass and biomass combustion-C14 for source identification, chemical tracer
431 development, and model validation. *Nuclear Instruments & Methods in Physics Research Section*
432 *B-Beam Interactions with Materials and Atoms* 92(1-4): 404-409.
- 433 Davies, S. J., & Unam, L. (1999). Smoke-haze from the 1997 Indonesian forest fires: effects on
434 pollution levels, local climate, atmospheric CO₂ concentrations, and tree photosynthesis. *Forest*
435 *Ecology and Management*, 124(2-3): 137-144.
- 436 Draxler, R. R. a. R., G.D. (2013). HYSPLIT (HYbrid Single-Particle Lagrangian Integrated Trajectory)
437 Model access via NOAA ARL READY Website (<http://ready.arl.noaa.gov/HYSPLIT.php>). NOAA
438 Air Resources Laboratory, Silver Spring, MD.
- 439 Dvorska, A., Lammel, G., & Holoubek, I. (2009). Recent trends of persistent organic pollutants in air
440 in central Europe - Air monitoring in combination with air mass trajectory statistics as a tool to
441 study the effectivity of regional chemical policy. *Atmospheric Environment*, 43(6):1280-1287.
- 442 Erel, Y., Kalderon-Asael, B., Dayan, U., & Sandler, A. (2007). European atmospheric pollution
443 imported by cooler air masses to the Eastern Mediterranean during the summer. *Environmental*
444 *Science and Technology*, 41(15): 5198-5203.
- 445 Geresdi, I., Meszaros, E., & Molnar, A. (2006). The effect of chemical composition and size
446 distribution of aerosol particles on droplet formation and albedo of stratocumulus clouds.
447 *Atmospheric Environment*, 40(10): 1845-1855.
- 448 Gnanaseelan, C., & Vaid, B. H. (2010). Interannual variability in the Biannual Rossby waves in the
449 tropical Indian Ocean and its relation to Indian Ocean Dipole and El Nino forcing. *Ocean Dynamics*,
450 60(1):27-40.

451 Gras, J. L., Jensen, J. B., Okada, K., Ikegami, M., Zaizen, Y., & Makino, Y. (1999). Some optical
452 properties of smoke aerosol in Indonesia and tropical Australia. *Geophysical Research Letters*,
453 26(10): 1393-1396.

454 He, J., & Balasubramanian, R. (2008). Rain-aerosol coupling in the tropical atmosphere of Southeast
455 Asia: distribution and scavenging ratios of major ionic species. *Journal of Atmospheric Chemistry*,
456 60(3): 205-220.

457 He, J., Zielinska, B., & Balasubramanian, R. (2010). Composition of semi-volatile organic compounds
458 in the urban atmosphere of Singapore: influence of biomass burning. *Atmospheric Chemistry and
459 Physics*, 10(23): 11401-11413.

460 Heil, A., & Goldammer, J. G. (2001). Smoke-haze pollution: a review of the 1997 episode in Southeast
461 Asia. *Regional Environmental Change*, 2(1): 24-37.

462 Hu, Y., Odman, M. T., Chang, M. E., Jackson, W., Lee, S., Edgerton, E. S., et al. (2008). Simulation of
463 air quality impacts from prescribed fires on an urban area. *Environmental Science & Technology*,
464 42(10): 3676-3682.

465 IPCC (2007). Climate change 2007: the physical science basis. *Agenda*, 6(07).

466 Jacobson, M. Z. (2004). The short-term cooling but long-term global warming due to biomass burning.
467 *Journal of Climate*, 17(15): 2909-2926.

468 Jakubczyk, D., Zientara, M., Derkachov, G., Kolwas, K., & Kolwas, M. (2005). Light scattering by
469 microdroplets of water and water suspensions. In J. Kwela, R. Drozdowski, & T. J. Wasowicz
470 (Eds.), *5th Workshop on Atomic and Molecular Physics*. 5849: 62-69.

471 Kulmala, M., Vehkamäki, H., Petäjä, T., Dal Maso, M., Lauri, A., Kerminen, V.-M., et al. (2004).
472 Formation and growth rates of ultrafine atmospheric particles: a review of observations. *Journal of
473 Aerosol Science*, 35(2):143-176.

474 Langmann, B., & Graf, H. (2003). Indonesian smoke aerosols from peat fires and the contribution from
475 volcanic sulfur emissions. *Geophysical Research Letters*, 30(11): 1547. doi:10.1029/2002gl016646.

476 Langmann, B., & Heil, A. (2004). Release and dispersion of vegetation and peat fire emissions in the
477 atmosphere over Indonesia 1997/1998. *Atmospheric Chemistry and Physics*, 4: 2145-2160.

478 Lee, K. H., Kim, Y. J., & Kim, M. J. (2006). Characteristics of aerosol observed during two severe
479 haze events over Korea in June and October 2004. *Atmos. Environ.* 40(27): 5146-5155.

480 Lyamani, H., Olmo, F., & Alados-Arboledas, L. (2008). Light scattering and absorption properties of
481 aerosol particles in the urban environment of Granada, Spain. *Atmos. Environ.* 42(11): 2630-2642.

482 Lyamani, H., Olmo, F., Alcántara, A., & Alados-Arboledas, L. (2006). Atmospheric aerosols during
483 the 2003 heat wave in southeastern Spain I: Spectral optical depth. *Atmospheric Environment*,
484 40(33): 6453-6464.

485 MSC (2001). Precursor contributions to ambient fine particulate matter in Canada : a report by the
486 Meteorological Service of Canada.

487 Olson, D. A., & Norris, G. A. (2005). Sampling artifacts in measurement of elemental and organic
488 carbon: Low-volume sampling in indoor and outdoor environments. *Atmospheric Environment*,
489 39(30): 5437-5445.

490 Page, S. E., Siegert, F., Rieley, J. O., Boehm, H. D. V., Jaya, A., & Limin, S. (2002). The amount of
491 carbon released from peat and forest fires in Indonesia during 1997. *Nature*. 420(6911): 61-65.

492 Pandis, S. N., & Seinfeld, J. H. (1998). Atmospheric chemistry and physics: From air pollution to
493 climate change. New York: Wiley.

494 Radzi bin Abas, M., Oros, D. R., & Simoneit, B. R. T. (2004). Biomass burning as the main source of
495 organic aerosol particulate matter in Malaysia during haze episodes. *Chemosphere*. 55(8): 1089-
496 1095.

497 Ramanathan, V., Chung, C., Kim, D., Bettge, T., Buja, L., Kiehl, J. T., et al. (2005). Atmospheric
498 brown clouds: Impacts on South Asian climate and hydrological cycle. *Proceedings of the National
499 Academy of Sciences of the United States of America*. 102(15): 5326-5333.

500 Reid, J. S., Koppmann, R., Eck, T. F., & Eleuterio, D. P. (2005). A review of biomass burning
501 emissions part II: intensive physical properties of biomass burning particles. *Atmospheric
502 Chemistry and Physics*, 5: 799-825.

503 Rolph, G. D. (2013). Real-time Environmental Applications and Display sYstem (READY) Website
504 (<http://ready.arl.noaa.gov>). NOAA Air Resources Laboratory, Silver Spring, MD. .

505 See, S. W., Balasubramanian, R., & Wang, W. (2006). A study of the physical, chemical, and optical
506 properties of ambient aerosol particles in Southeast Asia during hazy and nonhazy days. *Journal of
507 Geophysical Research-Atmospheres*, 111(D10): doi:10.1029/2005jd006180.

508 Stohl, A. (1998). Computation, accuracy and applications of trajectories - A review and bibliography.
509 *Atmospheric Environment*, 32(6):947-966.

- 510 Stohl, A., & Seibert, P. (1998). Accuracy of trajectories as determined from the conservation of
511 meteorological tracers. *Quarterly Journal of the Royal Meteorological Society*, 124(549): 1465-
512 1484.
- 513 Sundarambal, P., Balasubramanian, R., Tkalich, P., & He, J. (2010). Impact of biomass burning on
514 ocean water quality in Southeast Asia through atmospheric deposition: field observations.
515 *Atmospheric Chemistry and Physics*, 10(23):11323-11336.
- 516 Tang, I. N. (1996). Chemical and size effects of hygroscopic aerosols on light scattering coefficients.
517 *Journal of Geophysical Research-Atmospheres*, 101(D14): 19245-19250, doi:10.1029/96jd03003.
- 518 Ter-Avetisyan, S., Schnurer, M., Stiel, H., & Nickles, P. V. (2003). A high-density sub-micron liquid
519 spray for laser driven radiation sources. *Journal of Physics D-Applied Physics*, 36(19):2421-2426.
- 520 Van der Werf, G. R., Dempewolf, J., Trigg, S. N., Randerson, J. T., Kasibhatla, P. S., Gigliof, L.,
521 Murdiyarso, D., Peters, W., Morton, D. C., Collatz, G. J., Dolman, A. J., DeFries, R. S. (2008).
522 Climate Regulation of Fire Emissions and Deforestation in Equatorial Asia. *Proceedings of the*
523 *National Academy of Sciences of the United States of America*, 105(51), 20350-20355.
- 524 Wang, W. (2002). Field Investigation of Atmospheric Visibility in Singapore. A submission in partial
525 fulfillment for the degree of Master of Engineering, National University of Singapore.
- 526 Xu, J., Bergin, M., Yu, X., Liu, G., Zhao, J., Carrico, C., et al. (2002). Measurement of aerosol
527 chemical, physical and radiative properties in the Yangtze delta region of China. *Atmospheric*
528 *Environment*, 36(2):161-173.

529 **Figure Captions**

530

531 Figure 1 Daily mean Dust Track-corrected gravimetric mass concentrations measured
532 over the entire sampling period with the identification of smoke-haze events in 2009

533

534 Figure 2 Hotspot maps in SEA and representative 96-hrs (4-days) back trajectories of
535 air masses for the sampling period from August to November in Singapore.
536 Representative Hotspots maps during (a) the pre-haze period; (b) the smoke-haze
537 period; and (c) the post-haze period; backward trajectory clusters during (d) the pre-
538 haze period; (e) the smoke-haze period; and (f) the post-haze period; (Regional
539 hotspots maps were obtained from MODIS FIRMS Web Fire Mapper)

540

541 Figure 3 Diurnal comparisons of hourly mean values for the (a) particle number
542 concentration (PNC), (b) particle surface area concentration (PSAC), and (c) particle
543 gravimetric mass concentration (PGMC) during clear (background air) and smoke-
544 haze affected days at the sampling site

545 Table 1: Statistical parameters of particle number and surface area concentrations
 546 measured during non-haze and haze affected days at the sampling site
 547

Diameter (nm)	0 – 50 nm		51 – 100 nm		101 – 560 nm		0 – 560 nm	
	dN/dlogD _p (#/cm ³)							
	Non-haze	haze	Non-haze	haze	Non-haze	Haze	Non-haze	haze
Mean	1.76E+05	1.89E+05	1.23E+05	9.81E+04	2.87E+04	5.11E+04	3.27E+05	3.38E+05
Median	1.73E+05	1.68E+05	1.29E+05	9.58E+04	2.93E+04	5.23E+04	3.26E+05	3.34E+05
SD	4.24E+04	7.86E+04	2.10E+04	2.24E+04	3.28E+03	7.71E+03	6.13E+04	9.29E+04
Min	1.29E+05	9.62E+04	9.06E+04	6.21E+04	2.30E+04	4.05E+04	2.48E+05	2.18E+05
Max	2.65E+05	3.59E+05	1.52E+05	1.37E+05	3.33E+04	6.14E+04	4.43E+05	5.37E+05
	dS/dlogD _p (nm ² /cm ³)							
	Non-haze	haze	Non-haze	haze	Non-haze	Haze	Non-haze	haze
Mean	5.64E+08	5.08E+08	1.85E+09	1.57E+09	2.32E+09	4.30E+09	4.73E+09	6.38E+09
Median	5.60E+08	5.05E+08	1.93E+09	1.54E+09	2.37E+09	4.43E+09	4.94E+09	6.31E+09
SD	1.12E+08	1.87E+08	3.08E+08	3.22E+08	2.63E+08	8.46E+08	4.89E+08	5.99E+08
Min	4.34E+08	2.76E+08	1.35E+09	1.04E+09	1.94E+09	2.89E+09	3.74E+09	5.38E+09
Max	7.63E+08	9.14E+08	2.26E+09	2.12E+09	2.79E+09	5.42E+09	5.28E+09	7.37E+09

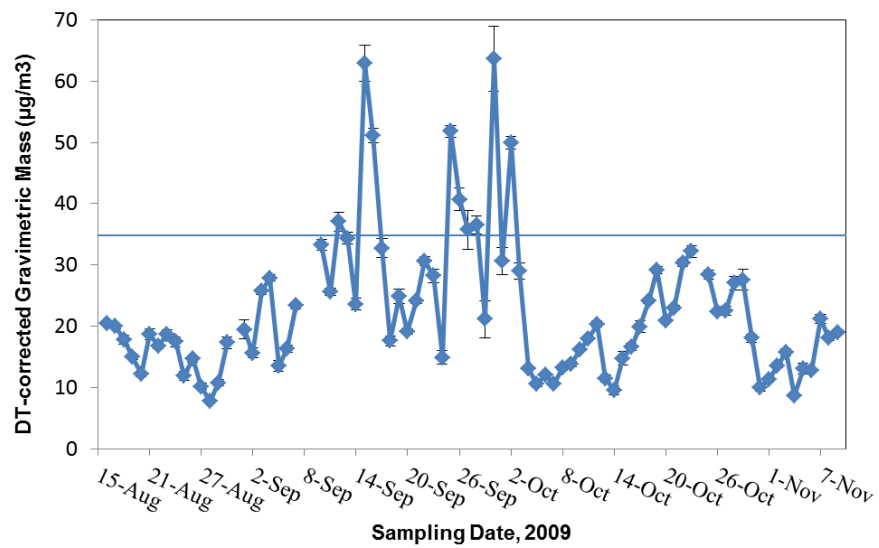
548 *SD (Standard deviation) over the 24-hrs diurnal sampling period

549 Table 2: Summary of temporal variations of mean mass concentrations of inorganic
 550 water-soluble ions measured over the entire sampling period (pre-haze, smoke-haze,
 551 post-haze periods)

		Anions ($\mu\text{g m}^{-3}$)				Cations ($\mu\text{g m}^{-3}$)			
		Cl ⁻	NO ₃ ⁻	SO ₄ ²⁻	nss- SO ₄ ²⁻	Na ⁺	NH ₄ ⁺	K ⁺	nss- K ⁺
Pre- Haze	Mean	2.97	0.54	2.85	2.42	1.72	0.15	0.48	0.42
	SD*	0.55	0.09	–	0.87	0.70	0.08	0.09	–
Smoke- Haze	Mean	2.50	0.81	4.93	4.20	2.92	0.50	0.60	0.49
	SD	0.61	0.44	–	1.56	0.75	0.41	0.32	–
Post- Haze	Mean	2.65	0.43	2.60	2.27	1.33	0.16	0.28	0.23
	SD	0.48	0.20	–	1.23	0.84	0.27	0.07	–

552 *SD: standard deviation

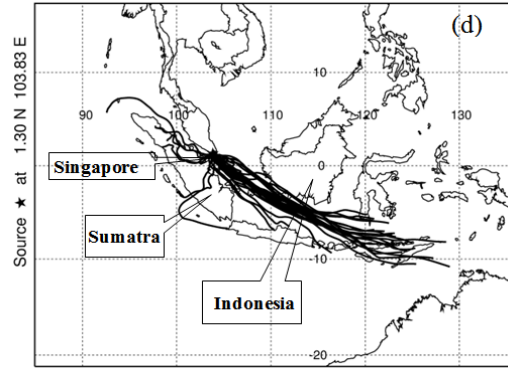
553



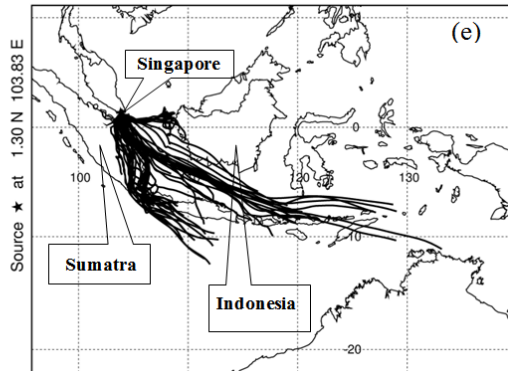
554

555 Figure 1 Daily mean Dust Track-corrected gravimetric mass concentrations measured
556 over the entire sampling period with the identification of smoke-haze events in 2009
557

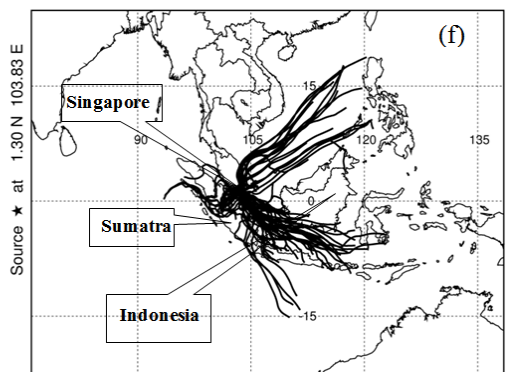
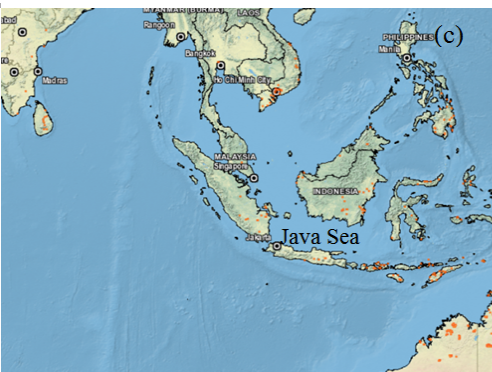
558



559



560

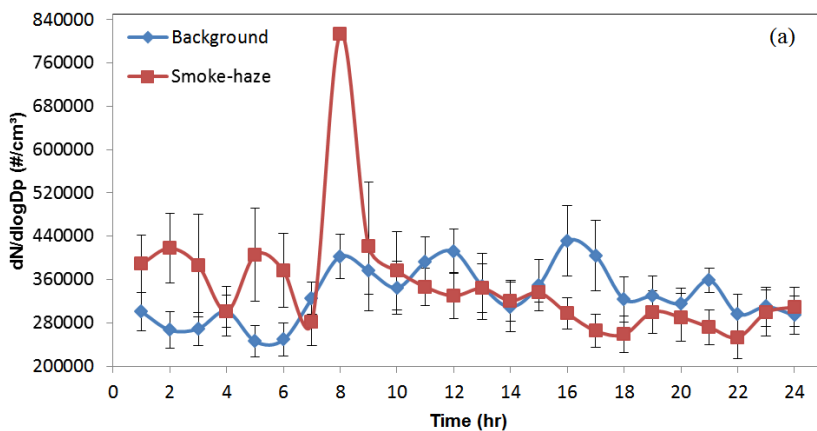


561

562 Figure 2 Hotspot maps in SEA and representative 96-hrs (4-days) back trajectories of
 563 air masses for the sampling period from August to November in Singapore.
 564 Representative Hotspots maps during (a) the pre-haze period; (b) the smoke-haze
 565 period; and (c) the post-haze period; backward trajectory clusters during (d) the pre-
 566 haze period; (e) the smoke-haze period; and (f) the post-haze period; (Regional
 567 hotspots maps were obtained from MODIS FIRMS Web Fire Mapper)

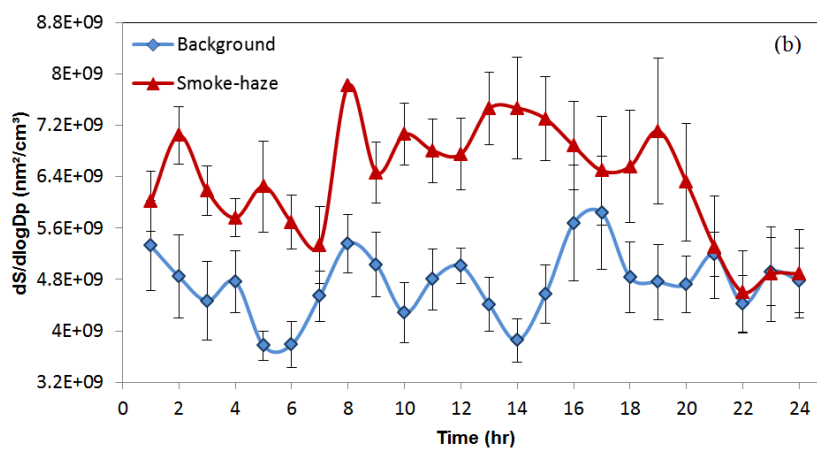
568

569



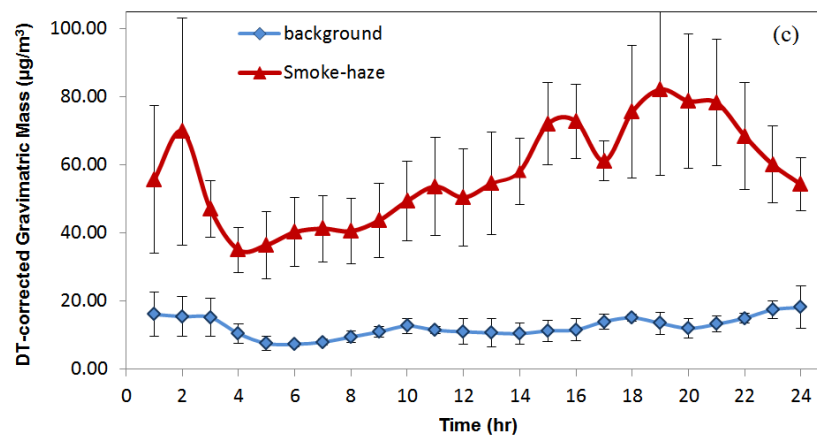
570

571



572

573



574

575

576 Figure 3 Diurnal comparisons of hourly mean values for the (a) particle number
577 concentration (PNC), (b) particle surface area concentration (PSAC), and (c) particle
578 gravimetric mass concentration (PGMC) during clear (background air) and smoke-
579 haze affected days at the sampling site